

Impact of improved energy resolution on DUNE sensitivity in presence of a light sterile neutrino

Sabila Parveen^{§ a}, Jogesh Rout^{¶ b} and Poonam Mehta^{§ c}

[§] *School of Physical Sciences, Jawaharlal Nehru University, New Delhi 110067, India*

[¶] *Department of Physics, Shree Ram College, Rampur, Subarnapur, Odisha 767045, India*

Abstract

The Deep Underground Neutrino Experiment (DUNE) primarily aims to measure the yet unknown parameters of the standard three neutrino framework, i.e., the determination of Dirac CP phase (δ_{13}), neutrino mass hierarchy (MH) and octant of θ_{23} . In the present work, we consider the standard three neutrino paradigm (referred to as the $(3+0)$ case) and beyond with an additional light sterile neutrino (referred to as the $(3+1)$ case). We consider two configurations : standard energy resolution as in DUNE Technical Design Report (TDR) and improved energy resolution and study the impact of energy resolution in the $(3+0)$ and $(3+1)$ cases. In general, inclusion of subdominant new physics effects spoils the sensitivities. However, improved energy resolution leads to enhancement in sensitivities to the three unknowns in both $(3+0)$ and $(3+1)$ cases.

arXiv:2506.10767v1 [hep-ph] 12 Jun 2025

^aEmail: sabila41_sps@jnu.ac.in

^bEmail: johesh.rout1@gmail.com

^cEmail: pm@jnu.ac.in

1 Introduction

The immense progress over the past few decades in neutrino physics with various ongoing and upcoming efforts has opened up possibilities of probing physics beyond the Standard Model (BSM) with neutrinos. The wealth of data accumulated from a series of oscillation experiments using solar, atmospheric, accelerator and reactor neutrinos in past few decades have established beyond doubt that neutrinos oscillate among the three flavor while conserving the lepton number [1] (for global analyses of neutrino data, see [2–4]). The neutrino oscillation experiments are sensitive only to the mass-squared differences (but not the absolute masses). There are several remaining questions at the present juncture and in the present work, we shall explore some of the yet unresolved questions such as establishing the presence (or absence) of CP violation in the leptonic sector, determining the neutrino MH and the correct octant of θ_{23} .

The question of whether CP in the leptonic sector is violated or not is a fundamental one and could have a bearing on matter-antimatter asymmetry of the universe [5]. The issue of determining the hierarchy of neutrino masses m_i , with $i = 1, 2, 3$, refers to finding the ordering of the mass eigenstates. The present oscillation data (i.e., the smaller mass-squared difference $\Delta m_{21}^2 = m_2^2 - m_1^2 > 0$ and the absolute value of the larger mass-squared splitting, $|\Delta m_{31}^2| = |m_3^2 - m_1^2|$) indicates a hierarchical pattern of neutrino masses and one can have the following two possibilities : normal hierarchy (NH) when sign of $\Delta m_{31}^2 > 0$ or inverted hierarchy (IH) when sign of $\Delta m_{31}^2 < 0$. Likewise, if θ_{23} is not maximal, the question of the octant of θ_{23} refers to finding the correct octant of θ_{23} ($\theta_{23} < \pi/4$ is the lower octant (LO) and $\theta_{23} > \pi/4$ is the higher octant (HO)).

Despite tremendous progress in our understanding of neutrino mass and mixing from several experiments, there are hints pointing towards physics BSM. If true, such hints could drastically impact our understanding/interpretation of neutrino mass and mixings. One such hint comes from a class of experiments referred to as the short baseline experiments. It was suggested that there could be oscillations driven by additional sterile neutrino state with mass-squared differences of order 1 eV^2 [6, 7]. The oscillations driven by 1 eV^2 mass splitting could leave their imprints at long baselines, thereby impacting the clean extrication of the unknowns in the neutrino oscillation physics.

The first hint in favor of sterile neutrino came from the Liquid Scintillator Neutrino Detector (LSND), which reported an excess of $\bar{\nu}_e$ events with a significance of 3.8σ [8]. This observation was later supported by the MiniBooNE experiment, which reported the excess at 4.8σ significance [9]. The combined significance of the LSND and MiniBooNE brought the excess was around 6.1σ [9]. Further, MicroBooNE experiment reported no evidence in support of the existence of the eV-scale sterile neutrino [10]. A combined analysis of MiniBooNE and MicroBooNE data suggested a preference for oscillations involving three active and one sterile neutrino state [11]. It should also be noted that Gallium-based radiochemical experiments designed to study solar neutrinos, such as SAGE [12], GALLEX [13], and the Baksan Experiment on Sterile Transition (BEST) [14], observed a deficit in ν_e events at a significance greater than 3σ , providing hints of $\nu_e \rightarrow \nu_s$ oscillation with mass-squared difference, $\Delta m_{41}^2 \sim 1 \text{ eV}^2$. Similar support came from the reactor anti-neutrino anomaly (RAA) [15, 16] and several experiments have been planned to test this anomaly. The Reactor-based Neutrino-4 experiment supported the active-sterile oscil-

lation with $\Delta m_{41}^2 \sim 7 \text{ eV}^2$ and $\sin^2 \theta_{14} \sim 0.09$ at 3σ confidence level (C.L.) [17]. In future, the Short Baseline Neutrino (SBN) program [18] at Fermilab comprising of three detectors, Short-Baseline Near Detector (SBND) [19], MicroBooNE [10] and Short-Baseline Far Detector (SBFD) [20] is expected to clarify the situation regarding the existence of eV-scale sterile neutrino.

There are several competing and complimentary long baseline experiments (with $L/E \sim \mathcal{O}(500) \text{ km/GeV}$) that aim to improve the precision on measured parameters as well as to resolve some of the open questions in neutrino oscillation physics, for instance, Tokai to Hyper-Kamiokande (T2HK) [21] in Japan with a baseline of 295 km and peak neutrino energy of $\sim 0.6 \text{ GeV}$, Deep Underground Neutrino Experiment (DUNE) with a baseline of 1300 km and peak neutrino energy of $\sim 2.5 \text{ GeV}$ [22,23] and Protvino to Orca (P2O) [24,25] with a baseline of 2595 km and peak neutrino energy of $\sim 5.1 \text{ GeV}$.

A lot of effort has gone into studies pertaining to theoretical and phenomenological implications of an eV-scale sterile neutrino on signals at long baseline experiments [26–41]. In earlier work involving some of the authors, we have addressed the question of separating between the $(3+0)$ and $(3+1)$ scenarios at different long baseline experiments such as T2HK, DUNE and P2O [40]. We also showed that DUNE will set competitive constraints on the parameter space of active-sterile mixing parameters by using various experimental configurations such as high energy beam tunes - low energy (LE) and medium energy (ME), near detector (ND), far detector (FD), charged current (CC) interactions and neutral current (NC) interactions etc [41]. Most of these studies consider the energy resolution to be the standard as given in the technical reports of the respective experiments.

In the present study, we consider two physics scenarios : three active neutrinos i.e., the $(3+0)$ case and three active plus one sterile neutrino i.e., the $(3+1)$ case. We take into account improved energy resolution [42,43] over and above the one detailed in DUNE Technical Design Report (TDR) [22,23] and demonstrate its impact on sensitivities to standard unknowns. The impact of energy resolution on a particular new physics scenario of neutrino non-standard interactions (NSI) has been explored in [43]. Our findings show that better neutrino energy resolution significantly enhances the DUNE sensitivity in both the considered scenarios. The improved energy resolution leads to a better reconstruction particularly in the neighbourhood of first oscillation peak of DUNE.

The plan of the article is as follows. In Sec. 2, we provide analytical discussion in $(3+0)$ and $(3+1)$ case with probability differences for CP violation and MH for the relevant appearance and disappearance channels. Sec 3 provides details of the experiment and simulation with details about energy resolution. In Sec. 4, we give event rates obtained using DUNE TDR and best reconstruction scenario. Sec. 5 provides details of the χ^2 sensitivities for the three unknowns : CP violation, MH and octant of θ_{23} . The results and discussions are presented in Sec. 6. We summarize in Sec. 7.

2 Theoretical framework

2.1 Hamiltonian in the (3 + 0) case

In the three flavor framework, the neutrino mixing matrix in the commonly adopted Pontecorvo–Maki–Nakagawa–Sakata (PMNS) form is [44–48]

$$\mathcal{U} = \begin{pmatrix} c_{12}c_{13} & s_{12}c_{13} & s_{13}e^{-i\delta_{13}} \\ -s_{12}c_{23} - c_{12}s_{13}s_{23}e^{i\delta_{13}} & c_{12}c_{23} - s_{12}s_{13}s_{23}e^{i\delta_{13}} & c_{13}s_{23} \\ s_{12}s_{23} - c_{12}s_{13}c_{23}e^{i\delta_{13}} & -c_{12}s_{23} - s_{12}s_{13}c_{23}e^{i\delta_{13}} & c_{13}c_{23} \end{pmatrix} \begin{pmatrix} 1 & & \\ & e^{i\phi_1} & \\ & & e^{i\phi_2} \end{pmatrix}, \quad (1)$$

where, $c_{ij} = \cos\theta_{ij}$ and $s_{ij} = \sin\theta_{ij}$. Note that only the Dirac phase (δ_{13}) affects neutrino oscillations and the two Majorana phases (ϕ_1 and ϕ_2) have no effect on neutrino oscillations.

We can write down the effective Hamiltonian in flavor basis as

$$\mathcal{H} = \mathcal{U} \left[\frac{1}{2E} \begin{pmatrix} 0 & 0 & 0 \\ 0 & \alpha & 0 \\ 0 & 0 & 1 \end{pmatrix} \right] \mathcal{U}^\dagger + \begin{pmatrix} V_{CC} & 0 & 0 \\ 0 & 0 & 0 \\ 0 & 0 & 0 \end{pmatrix}, \quad (2)$$

where, $\Delta m_{21}^2 = m_2^2 - m_1^2$, $\Delta m_{31}^2 = m_3^2 - m_1^2$, and $\alpha = \Delta m_{21}^2/\Delta m_{31}^2$. V_{CC} is the matter-induced potential due to the standard CC interactions of ν_e with electrons, given by

$$V_{CC} = \sqrt{2}G_F N_e = 7.6 \times 10^{-14} Y_e \left[\frac{\rho}{\text{g/cc}} \right] \text{eV},$$

where G_F is the Fermi coupling constant and $N_e = N_{\text{Avo}} \rho Y_e$ is the electron number density, ρ is the mass density, $N_{\text{Avo}} = 6.023 \times 10^{23} \text{g}^{-1} \text{mole}^{-1}$ is the Avogadro's number and $Y_e \simeq 0.5$ is the number of electrons per nucleon.

2.2 Hamiltonian for the (3 + 1) case

In the (3+1) framework, the mixing matrix \mathcal{U} is a 4×4 unitary matrix (different parameterizations have been used in literature such as [49–51]). In the present work, we adopt the notation [50].

$$\mathcal{U} = V(\theta_{34}, \delta_{34})O(\theta_{24})V(\theta_{14}, \delta_{14})O(\theta_{23})V(\theta_{13}, \delta_{13})O(\theta_{12}),$$

where, $V(\theta_{ij}, \delta_{ij})$ and $O(\theta_{ij})$ are complex and real rotation matrices in the i - j plane respectively (with $i, j = 1, 2, 3, 4$ and $i \neq j$).

The effective Hamiltonian for the (3 + 1) case in flavor basis is

$$\mathcal{H} = \mathcal{U} \left[\frac{1}{2E} \begin{pmatrix} 0 & 0 & 0 & 0 \\ 0 & \alpha & 0 & 0 \\ 0 & 0 & 1 & 0 \\ 0 & 0 & 0 & R \end{pmatrix} \right] \mathcal{U}^\dagger + \begin{pmatrix} V_{CC} + V_{NC} & 0 & 0 & 0 \\ 0 & V_{NC} & 0 & 0 \\ 0 & 0 & V_{NC} & 0 \\ 0 & 0 & 0 & 0 \end{pmatrix}, \quad (3)$$

where $R = \Delta m_{41}^2/\Delta m_{31}^2$ is a dimensionless quantity and $V_{NC} = -\sqrt{2}G_F N_n/2$ is the NC potential. Note that in the (3 + 1) framework, there are three new angles ($\theta_{14}, \theta_{24}, \theta_{34}$), two new phases (δ_{14}, δ_{34}) and one additional squared-mass difference Δm_{41}^2 .

In what follows, we present observables to quantify CP violation and MH in the two scenarios.

2.3 CP violating probability differences for the (3 + 0) and (3 + 1) cases

The CP violating probability difference is given by

$$\Delta P_{\alpha\beta}^{CP} = P_{\alpha\beta} - \bar{P}_{\alpha\beta}, \quad (4)$$

where $P_{\alpha\beta}$ is the probability for $\nu_\alpha \rightarrow \nu_\beta$ and $\bar{P}_{\alpha\beta}$ is the probability for antineutrinos.

We use some approximations for calculating the $\Delta P_{\mu e}^{CP}$ in the (3+1) case as mentioned in [50]. We average over oscillations induced by the largest mass-squared difference, Δm_{41}^2 . Since $\theta_{13}, \theta_{14}, \theta_{24} \leq 13^\circ$ [52], we have set $\sin \theta_{ij} \sim 10^{-1} \sim \lambda$, where θ_{ij} could be θ_{13}, θ_{14} or θ_{24} .

For the appearance channel ($\nu_\mu \rightarrow \nu_e$), we have

$$\begin{aligned} \Delta P_{\mu e}^{CP(3+1)}(\theta_{14}, \theta_{24}) \simeq & \Delta P_{\mu e}^{CP(3+0)} + 4s_{13}s_{14}s_{24}s_{23} \left\{ \sin[\delta_{13} - \delta_{14}] \left[\frac{\sin[\hat{A} - 1]\Delta}{(\hat{A} - 1)} \cos[(1 - \hat{A})\Delta] \right. \right. \\ & + \left. \frac{\sin[\hat{A} + 1]\Delta}{(\hat{A} + 1)} \cos[(1 + \hat{A})\Delta] \right] + \cos[\delta_{13} - \delta_{14}] \left[\frac{\sin[\hat{A} - 1]\Delta}{(\hat{A} - 1)} \sin[(1 - \hat{A})\Delta] \right. \\ & \left. \left. - \frac{\sin[\hat{A} + 1]\Delta}{(\hat{A} + 1)} \sin[(1 + \hat{A})\Delta] \right] \right\} + \mathcal{O}(\lambda^4), \quad (5a) \end{aligned}$$

Note that the expression for $P_{\mu e}^{CP(3+0)}$ is given in Appendix A. For the disappearance channel ($\nu_\mu \rightarrow \nu_\mu$), we have

$$\begin{aligned} \Delta P_{\mu\mu}^{CP(3+1)}(\theta_{14}, \theta_{24}) \simeq & \Delta P_{\mu\mu}^{CP(3+0)} + \frac{1}{4}s_{13}s_{14}s_{24}c_{24} \left\{ -s_{23} \left[\frac{\cos[\delta_{14} + (\hat{A} - 1)\Delta]}{\hat{A} - 1} \right. \right. \\ & + \left. \frac{\cos[\delta_{14} + (\hat{A} + 1)\Delta]}{\hat{A} + 1} \right] + \frac{2\hat{A}}{\hat{A} - 1} s_{23} \cos[\delta_{14} + 2\hat{A}\Delta] \\ & + 2 \sin[\delta_{13} + \delta_{14}] \sin 2\theta_{23} \left[\frac{\sin[2\Delta + \delta_{13}]}{\hat{A} + 1} - \frac{\sin[2\Delta - \delta_{13}]}{\hat{A} - 1} \right] + 2 \sin 3\theta_{23} \\ & \left[\frac{\cos[2\Delta - \delta_{13}] \cos[\delta_{14} - \delta_{13}/2 - \omega_-]}{\hat{A} - 1} + \frac{\cos[2\Delta + \delta_{13}] \cos[\delta_{14} - \delta_{13}/2 + \omega_+]}{\hat{A} + 1} \right] \\ & \left. + 2 \sin 4\theta_{23} \cos[\delta_{14} + \delta_{13}] \left[\cos(2\Delta - \delta_{13})\Omega_- + \cos(2\Delta + \delta_{13})\Omega_+ \right] \right\} \\ & + \frac{1}{2}s_{14}s_{13}s_{23}s_{24}c_{24} \left\{ \frac{\cos[\delta_{14} - 2\Delta]}{\hat{A} - 1} - \frac{\cos[\delta_{14} + 2\Delta]}{\hat{A} + 1} - \cos[\delta_{14} - \delta_{13}] \left(\frac{2\hat{A}}{\hat{A}^2 - 1} \right) \right. \\ & \left. + 2 \cos 2\theta_{23} \left[\Omega_- \cos[\delta_{14} - \Delta - \delta_{13}/2] + \Omega_+ \cos[\delta_{14} + \Delta - \delta_{13}/2] \right] \right\} + \mathcal{O}(\lambda^4), \quad (5b) \end{aligned}$$

where, we have used

$$\Delta = \frac{\Delta m_{31}^2 L}{4E}, \quad \hat{A} = \frac{A}{\Delta m_{31}^2}, \quad \Omega_\pm = \frac{\cos(\Delta \pm \delta_{13}/2)}{\hat{A} \pm 1}, \quad \omega_\pm = (1 \pm 2\hat{A})\Delta.$$

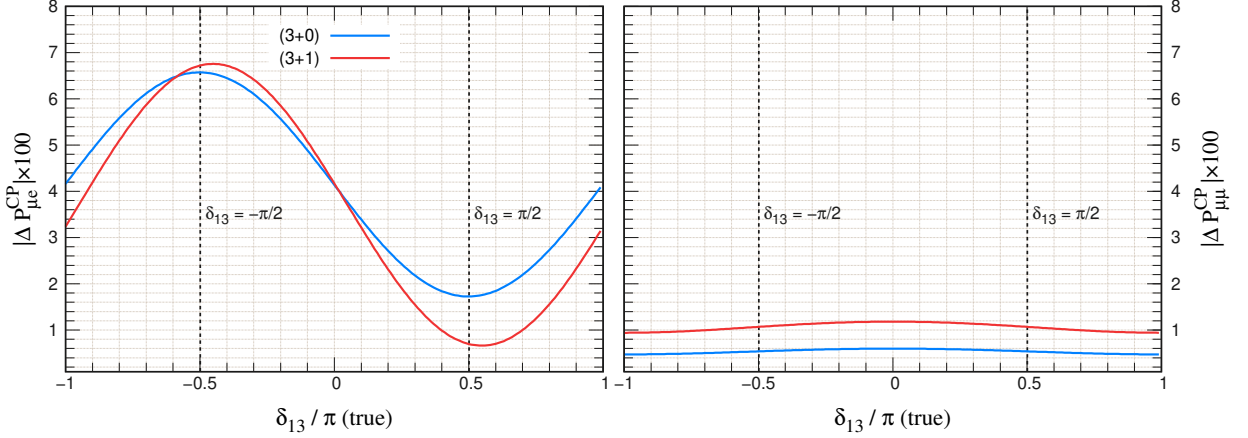


Figure 1: $|\Delta P_{\mu e}^{CP}|$ and $|\Delta P_{\mu\mu}^{CP}|$ plotted as a function of δ_{13} for $L = 1300$ km, $E = 2.6$ GeV. The (3 + 0) and (3 + 1) cases are depicted by blue and red curves respectively.

Note that the expression for $P_{\mu\mu}^{CP(3+0)}$ is given in Appendix A. We retain terms upto order $\mathcal{O}(\lambda^3)$. In the limiting case, when $(\theta_{14}, \theta_{24}, \theta_{34}, \delta_{14}, \delta_{34})$ tend to zero, we recover the corresponding probability differences in (3 + 0) case [40, 53].

In Fig 1, we plot the CP violating differences, i.e., $\Delta P_{\alpha\beta}^{CP}$, as a function of δ_{13} for $L = 1300$ km, $E = 2.6$ GeV for the two scenarios under consideration. The left panel is for $\nu_\mu \rightarrow \nu_e$ channel where as the right panel corresponds to $\nu_\mu \rightarrow \nu_\mu$ channel. The simulations have been performed using the software General Long Baseline Experiment Simulator (GLOBES) [54, 55] which solves the full three flavor neutrino propagation equations numerically using the Preliminary Reference Earth Model (PREM) [56] density profile of the Earth.

2.4 MH probability differences for the (3 + 0) and (3 + 1) cases

The MH probability difference is given by

$$\Delta P_{\alpha\beta}^{MH} = P_{\alpha\beta}^{NH} - P_{\alpha\beta}^{IH}, \quad (6)$$

where $P_{\alpha\beta}^{NH}$ is the probability for NH and $P_{\alpha\beta}^{IH}$ is the probability in case of IH. Analytic expressions for probability for NH are given in [50]. By replacing Δ with $-\Delta$, α with $-\alpha$ and \hat{A} with $-\hat{A}$ in the probability expressions for NH, we can obtain the expressions for IH. Thus, MH probability difference for the appearance channel ($\nu_\mu \rightarrow \nu_e$) is given by

$$\begin{aligned} \Delta P_{\mu e}^{MH(3+1)}(\theta_{14}, \theta_{24}) \simeq & \Delta P_{\mu e}^{MH(3+0)} + 4s_{13}s_{14}s_{24}s_{23} \left\{ \sin[\delta_{13} - \delta_{14}] \left[\frac{\sin[\hat{A} - 1]\Delta}{(\hat{A} - 1)} \cos[(1 - \hat{A})\Delta] \right. \right. \\ & + \left. \frac{\sin[\hat{A} + 1]\Delta}{(\hat{A} + 1)} \cos[(1 + \hat{A})\Delta] \right] + \cos[\delta_{13} - \delta_{14}] \left[\frac{\sin[\hat{A} - 1]\Delta}{(\hat{A} - 1)} \sin[(1 - \hat{A})\Delta] \right. \\ & \left. \left. - \frac{\sin[\hat{A} + 1]\Delta}{(\hat{A} + 1)} \sin[(1 + \hat{A})\Delta] \right] \right\} + \mathcal{O}(\lambda^4), \quad (7a) \end{aligned}$$

Parameter	Best-fit value	3σ interval	1σ uncertainty
$\theta_{12}/^\circ$	34.3	31.4 - 37.4	2.9%
$\theta_{13}/^\circ$	8.53 (8.58)	8.13 - 8.92 (8.17 - 8.96)	1.5%
$\delta_{13}/^\circ$	194 (284)	[128 - 359] ([200 - 353])	-
Δm_{31}^2 [eV ²]	$+2.55 (-2.45) \times 10^{-3}$	$[2.47 - 2.63] (- [2.37 - 2.53]) \times 10^{-3}$	1.2%
Δm_{21}^2 [eV ²]	7.5×10^{-5}	$[6.94 - 8.14] \times 10^{-5}$	2.7%
Δm_{41}^2 [eV ²]	1	-	-
$\theta_{14}/^\circ$	5.7	0 - 18.4	$\sigma(\sin^2 \theta_{14}) = 5\%$
$\theta_{24}/^\circ$	5	0 - 6.05	$\sigma(\sin^2 \theta_{24}) = 5\%$
$\theta_{34}/^\circ$	20	0 - 25.8	$\sigma(\sin^2 \theta_{34}) = 5\%$
$\delta_{14}/^\circ$	0	[-180, 180]	-
$\delta_{34}/^\circ$	0	[-180, 180]	-

Table 1: The values of the oscillation parameters and their uncertainties. The values of standard (3+0) parameters have been taken from the global fit analysis [2] while the sterile (3+1) parameter values have been chosen from [52]. If the 3σ upper and lower limit of a parameter is x_u and x_l respectively, the 1σ uncertainty is $(x_u - x_l)/3(x_u + x_l)\%$ [22]. For the active-sterile mixing angles, a conservative 5% uncertainty has been used on $\sin^2 \theta_{i4}$ ($i = 1, 2, 3$). The bracketed values correspond to the case when the hierarchy is inverted. All other parameter values are for NH.

It may be noted that the expression for $P_{\mu e}^{MH(3+0)}$ is given in Appendix A. For the disappearance channel ($\nu_\mu \rightarrow \nu_\mu$), we have

$$\begin{aligned}
\Delta P_{\mu\mu}^{MH(3+1)}(\theta_{14}, \theta_{24}) &\simeq \Delta P_{\mu\mu}^{MH(3+0)} + \frac{1}{4} s_{13} s_{14} s_{24} c_{24} \left\{ -3s_{23} \left[\frac{\cos[\delta_{14} + (\hat{A} - 1)\Delta]}{\hat{A} - 1} \right. \right. \\
&+ \left. \frac{\cos[\delta_{14} - (\hat{A} + 1)\Delta]}{\hat{A} + 1} \right] + \frac{2\hat{A}}{(\hat{A}^2 - 1)} s_{23} \cos[\delta_{14} + 2\hat{A}\Delta + \delta_{13}] - 2 \sin[\delta_{14} + \delta_{13}] \\
&\sin 2\theta_{23} \left[\frac{\sin[2\Delta - \delta_{13}]}{\hat{A} - 1} - \frac{\sin[2\Delta + \delta_{13}]}{\hat{A} + 1} \right] + 2 \sin 3\theta_{23} \\
&\left. \left[\frac{\cos[\delta_{14} - \omega_- - \delta_{13}/2] \cos[2\Delta - \delta_{13}]}{\hat{A} - 1} + \frac{\cos[\delta_{14} - \omega_+ - \delta_{13}/2] \cos[2\Delta + \delta_{13}]}{\hat{A} + 1} \right] \right\} \\
&+ 2 \cos[\delta_{14} + \delta_{13}] \sin 4\theta_{23} \left[\Omega_- \cos[2\Delta - \delta_{13}] + \cos[2\Delta + \delta_{13}] \Omega_+ \right] + \frac{1}{2} s_{14} s_{13} s_{23} s_{24} c_{24} \\
&\left\{ \left[\frac{\cos[\delta_{14} - 2\Delta]}{\hat{A} - 1} + \frac{\cos[\delta_{14} + 2\Delta]}{\hat{A} + 1} \right] - 2 \cos[\delta_{14} - \delta_{13}] \left[\Omega_- \cos[\delta_{14} - \Delta - \delta_{13}/2] \right. \right. \\
&\left. \left. + \Omega_+ \cos[\delta_{14} + \Delta - \delta_{13}/2] \cos 2\theta_{23} \right] \right\} + \mathcal{O}(\lambda^4). \tag{7b}
\end{aligned}$$

The expression for $P_{\mu\mu}^{MH(3+0)}$ is given in Appendix A. In Fig 2, we plot the MH probability differences, i.e., $\Delta P_{\alpha\beta}^{MH}$, as a function of δ_{13} for $L = 1300$ km, $E = 2.6$ GeV for the two scenarios under consideration.

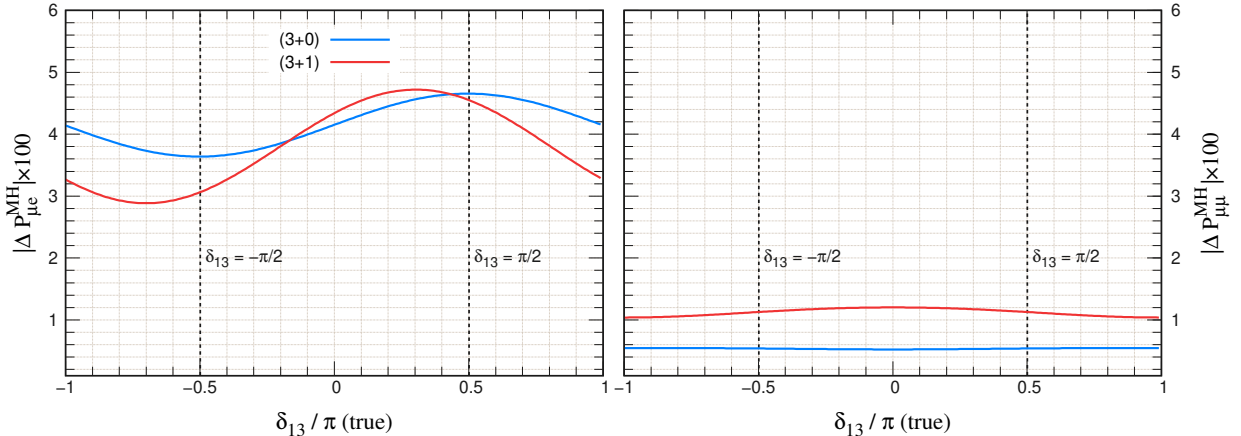


Figure 2: $|\Delta P_{\mu e}^{MH}|$ and $|\Delta P_{\mu\mu}^{MH}|$ plotted as a function of δ_{13} for $L = 1300$ km, $E = 2.6$ GeV. The (3 + 0) and (3 + 1) cases are depicted by blue and red curves respectively.

3 Details of the Experiment and Simulation

3.1 Experiment details

We use the latest configuration of the DUNE TDR [22, 23] in the present study. Neutrino beam originates at Fermi National Accelerator Laboratory (Fermilab) in Batavia, Illinois. The ND of DUNE, with a target mass of 0.067 kt, will be installed 570 m downstream. The FD, with a target mass of approximately 40 kt, will be located 1.5 km underground at the Sanford Underground Research Facility (SURF) in South Dakota, at a baseline of around 1300 km from the neutrino source. The DUNE experiment will utilize a 120 GeV proton beam of 1.2 MW power with total runtime of 13 years equally divided into neutrino and anti-neutrino mode. The total exposure is taken to be 624 kt·MW·years.

We use the standard LE beam which peaks around $\sim 2 - 3$ GeV Fig. 3. The neutrino beam is generated by directing a 120 GeV proton beam onto a graphite target. The resulting hadronic interactions are simulated using G4LBNF, a GEANT4-based framework [57, 58] developed for modeling the long baseline neutrino facility (LBNF) beamline [22]. The secondary hadrons produced in the target are focused by a system of three magnetic horns, each operating at a current of 300 kA. These hadrons are then allowed to decay within a 194 meter long, helium-filled decay pipe, yielding the LE neutrino flux. The focusing horns can be operated in forward and reverse current configurations to produce ν (solid blue) and $\bar{\nu}$ (dotted blue) beams respectively (see Fig. 3).

3.2 Simulation details

The simulations and sensitivity estimates have been carried out using the GLoBES software package [54, 55]. We numerically solve the full three flavor neutrino propagation equations assuming the Earth's matter density profile given by the Preliminary Reference Earth Model (PREM) [56].¹ For

¹Although it is possible to incorporate uncertainties in the Earth's matter density, previous studies [59–62] have shown that such variations have insignificant impact on the results.

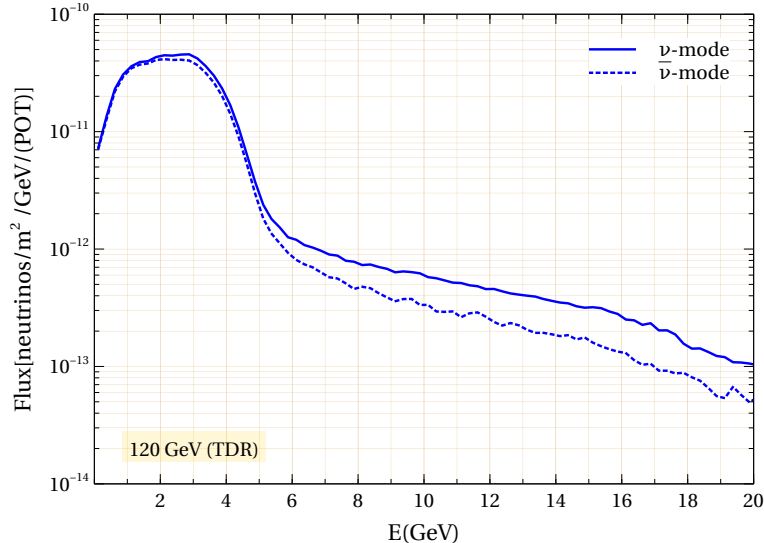


Figure 3: The blue curve represents the flux corresponding to DUNE TDR LE beam [22,23]. The solid and dotted curves indicate the ν_μ and $\bar{\nu}_\mu$ flux respectively.

true values of oscillation parameters, their 3σ ranges and corresponding uncertainties, we use the values given in Table 1. We assume a 2% uncertainty in the matter density [23] and marginalize over it when computing the minimum χ^2 .

3.3 Improved energy resolution

DUNE is based on liquid argon time projection chamber (LArTPC) technology [63]. The neutrino interacts with an argon nucleus in the neutrino detector and produces charged as well as neutral particles. The charged particles travel through the liquid argon and lose their energy through ionization and excitation of argon atoms. The ionized electrons propagate towards a set of anode wire planes under the influence of electric field and are finally collected. This charge deposition helps in obtaining showers and tracks which in turn leads to particle identification. The particle identification and energy deposition through the ionization together allows us to reconstruct the energy of individual particle, thereby allowing to infer the energy of the incoming neutrino.

In this work, we consider the parametrization used in [43] for the energy resolution function

$$R(E, E_r) = e^{-(E-E_r)^2/2\sigma^2} / \sigma\sqrt{2\pi}, \quad (8)$$

where E is the true neutrino energy, E_r is the reconstructed energy, and the energy resolution σ is given by

$$\sigma(E)/\text{GeV} = \alpha \cdot (E/\text{GeV}) + \beta \cdot \sqrt{E/\text{GeV}} + \gamma, \quad (9)$$

with fit parameters (α, β, γ) are $(0.045, 0.001, 0.048)$ for neutrinos and $(0.026, 0.001, 0.085)$ for antineutrinos (Fig. 4). These above values of fit parameters (α, β, γ) are obtained from the best reconstruction case given in [64].

In [64], a detailed simulation has been performed by identifying different channels where energy is lost or missed, such as sub-threshold particles, neutral particles like neutrons that deposit

energy inefficiently, energy consumed in nuclear processes, and charge recombination effects. Such energy losses cause fluctuations in the visible energy, which limit the achievable energy resolution. Therefore, improving particle identification, lowering detection thresholds, and accounting for charge recombination improves the energy resolution. The Fig. 4 presents the energy resolution for neutrinos (left panel) and anti-neutrinos (right panel) as a function of energy for the DUNE TDR case (blue curve) and the best reconstruction scenario (red curve).

In the present work, our focus is to consider improved energy resolution and study its impact on the sensitivities to current unknowns for the $(3 + 0)$ case and $(3 + 1)$ case at DUNE. For all the simulation studies pertaining to the best reconstruction case, we take the resolution for both appearance and disappearance channels to be the same. The migration matrices used for NC , ν_e contamination, misidentified muon, and $\nu_\mu \rightarrow \nu_\tau$ backgrounds are taken from [23].

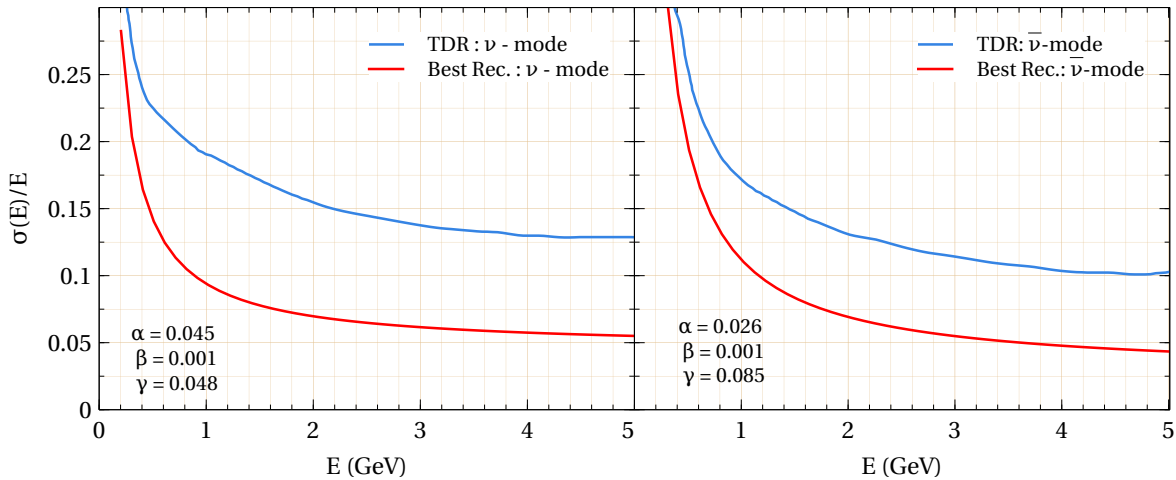


Figure 4: Energy resolution plotted as a function of neutrino energy. The blue and red curves depict the energy resolutions for DUNE TDR [22] and best reconstruction scenario respectively [43]. The left (right) panel corresponds to ν ($\bar{\nu}$) - mode.

4 Event rates

Theoretically, the expected event rate is given by

$$N_{\alpha\beta}(L) = N_{target} \times \int \Phi_{\nu_\alpha}(E, L) \times P_{\alpha\beta}(E, L) \times \sigma_{\nu_\beta}(E) dE, \quad (10)$$

where N_{target} is the number of target nucleons per kt of detector fiducial volume, for DUNE, $N_{target} = 6.022 \times 10^{32}$ N/kt where, N stands for the number of nucleons. $P_{\alpha\beta}(E, L)$ is the oscillation probability in matter, $\Phi_{\nu_\alpha}(E, L)$ is the flux of ν_α , $\sigma_{\nu_\beta}(E)$ is the CC cross section of ν_β . $\sigma_{\nu_e}(E)$ is given by [65, 66]

$$\sigma_{\nu_e}(E) = 0.67 \times 10^{-42} (m^2/\text{GeV}/N) \times E, \quad \text{for } E > 0.5 \text{ GeV}. \quad (11)$$

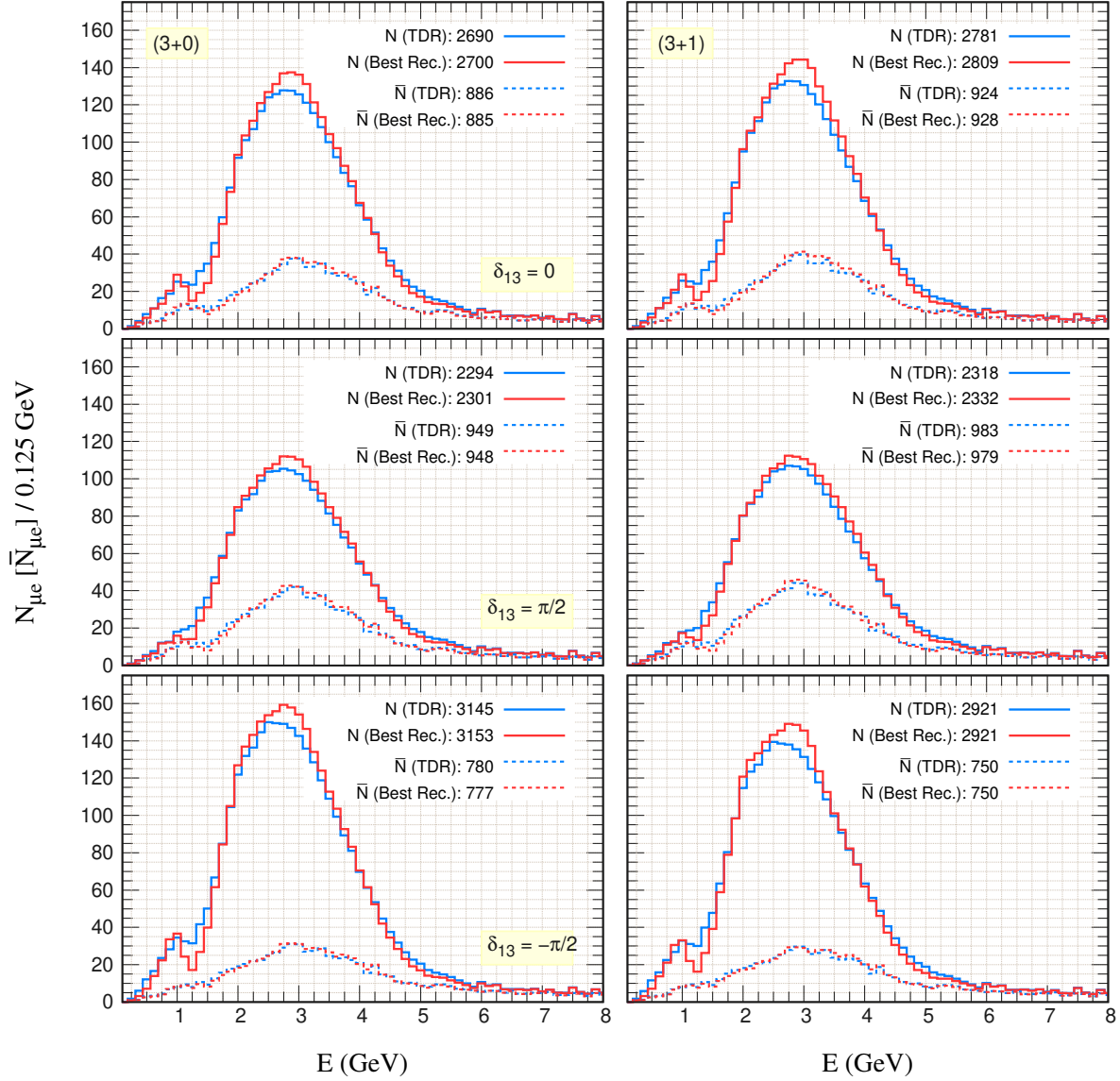


Figure 5: $N_{\mu e}$ ($\bar{N}_{\mu e}$) plotted as a function of energy for DUNE TDR and best reconstruction scenario for the (3 + 0) and (3 + 1) scenario at DUNE. The neutrino MH is assumed be NH.

It may be noted that $\sigma_{\nu_\mu} \sim \sigma_{\nu_e}$, for the energy range, 0 - 8 GeV [67]. For anti-neutrinos, the cross-section is roughly a factor of two smaller than the neutrinos [23]. To compute the events, we use the GLOBES software [54, 55]. The neutrino fluxes have been taken from DUNE TDR [23] (see Fig. 3).

We generate event rate as a function of energy for $\nu_\mu \rightarrow \nu_e$ ($\bar{\nu}_\mu \rightarrow \bar{\nu}_e$) and $\nu_\mu \rightarrow \nu_\mu$ ($\bar{\nu}_\mu \rightarrow \bar{\nu}_\mu$). The backgrounds include: (a) $\nu_\mu \rightarrow \nu_e/\nu_\tau$ and $\nu_\mu \rightarrow \nu_\mu$ CC in ν and $\bar{\nu}$ -mode and (b) $\nu_\mu/\nu_e \rightarrow X$ (NC) for appearance and disappearance channels (see details in [23]).

In Fig. 5 and Fig. 6, we present the event rates as a function of energy for TDR and best reconstruction scenario for $\nu_\mu \rightarrow \nu_e$ ($\bar{\nu}_\mu \rightarrow \bar{\nu}_e$) and $\nu_\mu \rightarrow \nu_\mu$ ($\bar{\nu}_\mu \rightarrow \bar{\nu}_\mu$) respectively. We consider three different values of CP phase, $\delta_{13} = 0$ (first row), $\delta_{13} = \pi/2$ (second row) and $\delta_{13} = -\pi/2$ (third row). We note the following:

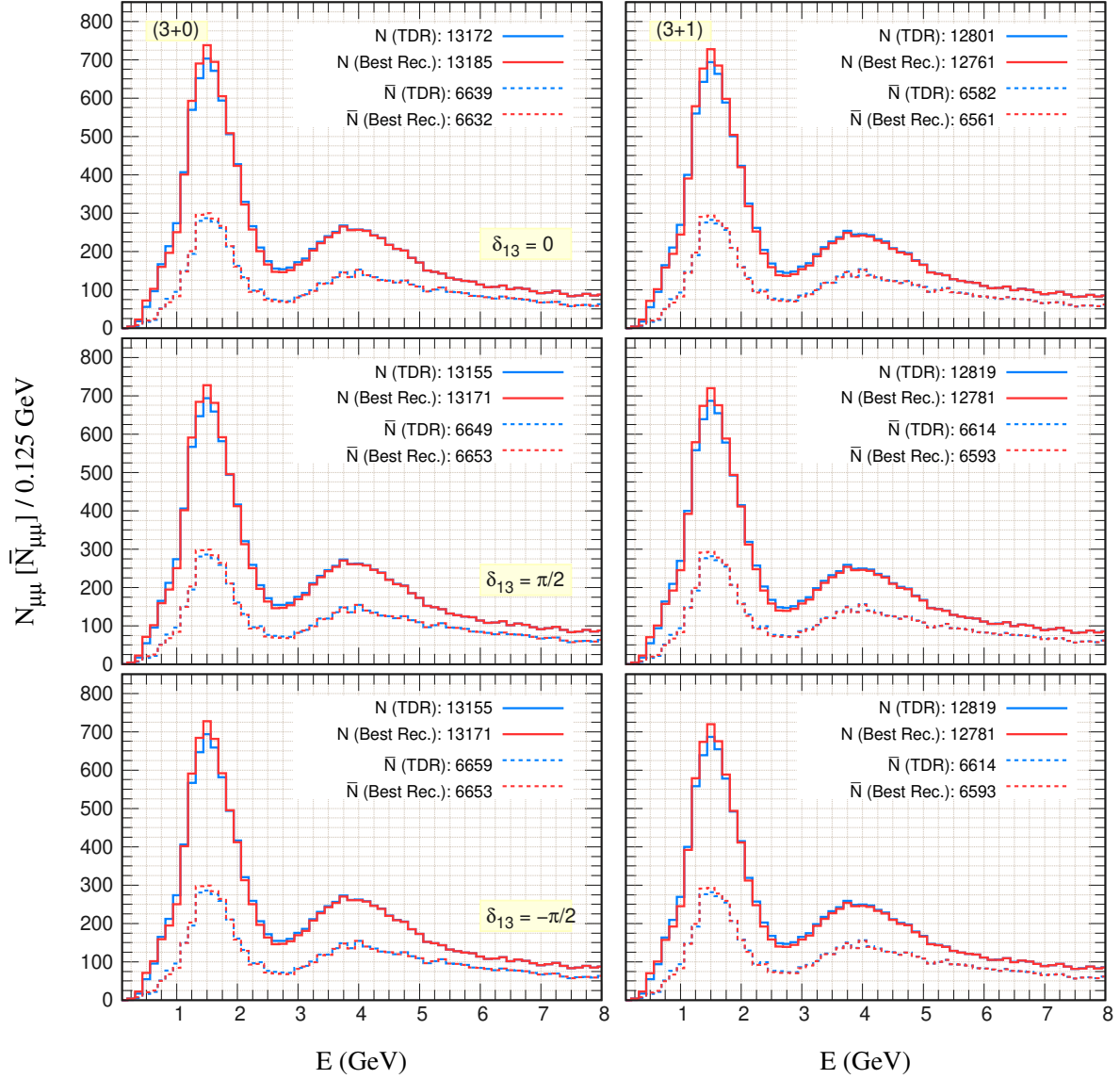


Figure 6: Same as Fig. 5 but for $\nu_{\mu} \rightarrow \nu_{\mu}$ ($\bar{\nu}_{\mu} \rightarrow \bar{\nu}_{\mu}$) channel.

- $\nu_{\mu} \rightarrow \nu_e$ ($\bar{\nu}_{\mu} \rightarrow \bar{\nu}_e$) channel: In Fig. 5, the event spectrum for the two cases (TDR and best reconstruction) has been plotted as a function of energy for (3+0) and (3+1) cases taking fixed values of $\delta_{13} = 0, \pm\pi/2$. It can be noted that better reconstruction leads to larger number of events for all values of δ_{13} . Larger deviation is seen in case of neutrinos for NH.
- $\nu_{\mu} \rightarrow \nu_{\mu}$ ($\bar{\nu}_{\mu} \rightarrow \bar{\nu}_{\mu}$) channel: In Fig. 6, the event spectrum for the two cases (TDR and best reconstruction) have been plotted as a function of energy for (3+0) and (3+1) cases taking fixed values of $\delta_{13} = 0, \pm\pi/2$. For $\delta_{13} = 0$, there is a difference between the (3+0) and (3+1) cases (~ 371 for TDR and ~ 424 for best reconstruction) in ν -mode and (~ 57 for TDR and ~ 71 for best reconstruction) in $\bar{\nu}$ -mode. As expected, for $\delta_{13} = \pm\pi/2$, the event rates are largely the same for TDR and best reconstruction case respectively.

5 Analysis procedure

To evaluate the sensitivities of DUNE to standard unknowns (CP violation, MH, and the octant of θ_{23}), we perform the standard χ^2 analysis. Although the results are primarily obtained through numerical computations using the GLOBES software, analytical expressions of χ^2 for each of these quantities allow us to understand the sensitivity estimates.

Sensitivity to CP violation:

Here we address the question of sensitivity of a given experiment to discriminate between CP conserving ($= 0, \pi$) and CP violating ($\neq 0, \pi$) values of the Dirac CP phase δ_{13} . Including only statistical effects, the χ^2 corresponding to CP violation sensitivity for a given oscillation channel is given by [68–70]

$$\chi^2 \equiv \min_{\delta_{test}} \sum_{i=1}^x \sum_{j=\nu, \bar{\nu}} \frac{\left[N_{true}^{i,j}(\delta_{true}) - N_{test}^{i,j}(\delta_{test} = 0, \pi) \right]^2}{N_{true}^{i,j}(\delta_{true})}, \quad (12)$$

where $N_{true}^{i,j}$ and $N_{test}^{i,j}$ represent the true and test datasets in the $\{i, j\}$ -th bin respectively. Since no statistical fluctuations are introduced in the simulated data, we define $\Delta\chi^2 = \chi^2$, following Pearson’s definition of χ^2 [71]. The label i stands for the energy bins, where $i = 1$ to x , and x is the total number of bins, specific to the experiment under consideration. For DUNE experiment, there are $x = 62$ energy bins each having a width of 0.125 GeV in the energy range of 0.5 - 8 GeV and 2 bins of width 1 GeV each in the range 8 - 10 GeV [23]. The label j is being summed over the ν and $\bar{\nu}$ -mode. To evaluate the χ^2 relevant to CP violation sensitivity, the test values of the CP violating phase δ_{13} are fixed at 0 or π . The χ^2 is then computed for all possible true values of (δ_{13}) within the full range $[-\pi, \pi]$.

In the analysis, marginalization is performed over all standard oscillation parameters (see Table 1) except for δ_{13} whose true value remains undetermined. Additionally, the total χ^2 is obtained by summing the contributions from two different oscillation channels: ($\nu_\mu \rightarrow \nu_e$ ($\bar{\nu}_\mu \rightarrow \bar{\nu}_e$)) and ($\nu_\mu \rightarrow \nu_\mu$ ($\bar{\nu}_\mu \rightarrow \bar{\nu}_\mu$)). Table 2 gives the detector configuration, efficiencies and systematic uncertainties used in our analysis.

Detector details of DUNE	Normalization error	
	Signal	Background
E_p : 120 GeV , L : 1300 km		
target mass (fiducial) : 40 kt	ν_e : 2%	ν_e : 5%
detector type : LArTPC	ν_μ : 5%	ν_μ : 5%
number of bins : 64		ν_τ : 20%
bin width : 0.125 GeV		NC : 10%
runtime (yr) : $6.5 \nu + 6.5 \bar{\nu}$		
$R_\mu = 0.20/\sqrt{E}$, $R_e = 0.15/\sqrt{E}$		

Table 2: Detector configuration, efficiencies and systematic uncertainties for DUNE.

Sensitivity to the MH:

The question of hierarchy of neutrino masses is a binary one i.e., the true hierarchy can be NH or IH. Here we address the following question. What is the sensitivity with which a particular experiment such as DUNE can distinguish between NH and IH. In order to understand the features

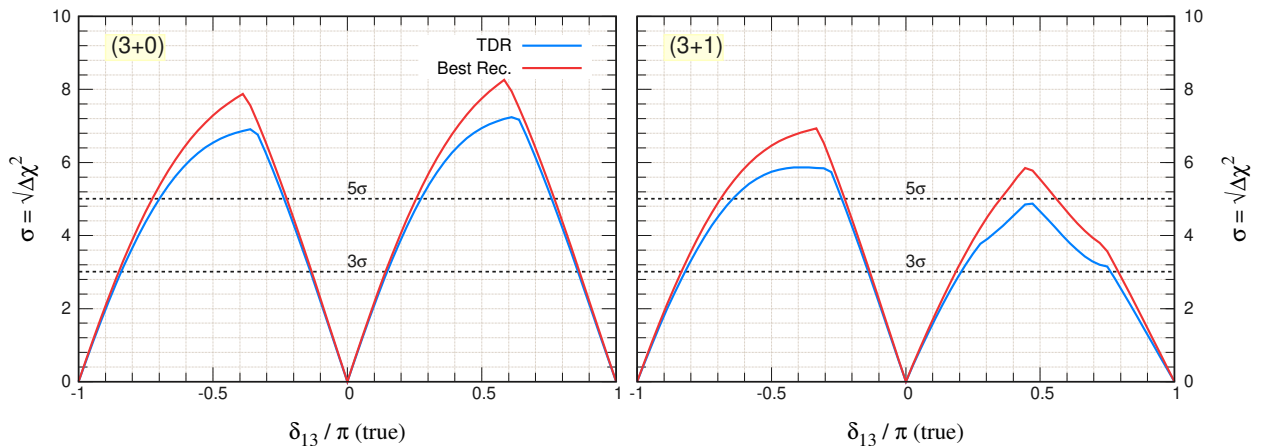


Figure 7: CP violation sensitivity as a function of δ_{13} for TDR (blue curve) and best reconstruction case (red curve) at DUNE. The left panel depicts the (3 + 0) case while the right panel depicts the (3 + 1) case.

of the sensitivity plots considering the true hierarchy as NH, we give a statistical definition of χ^2 as follows [66],

$$\chi^2 \equiv \min_{\delta_{test}} \sum_{i=1}^x \sum_{j=\nu, \bar{\nu}} \frac{[N_{NH}^{i,j}(\delta_{true}) - N_{IH}^{i,j}(\delta_{test})]^2}{N_{NH}^{i,j}(\delta_{true})}. \quad (13)$$

The quantities $N_{NH}^{i,j}$ and $N_{IH}^{i,j}$ denote the number of events in the i, j -th bin for the NH and IH respectively. The index i labels the energy bins, where $i = 1$ to x , and x is the total number of bins, specific to the experiment under consideration. For DUNE experiment, there are $x = 62$ energy bins each having a width of 0.125 GeV in the energy range of 0.5 - 8 GeV and 2 bins of width 1 GeV each in the range 8 - 10 GeV [23]. The index j accounts for summing over the mode (neutrino or antineutrino). The χ^2 (defined in Eq.(13)) is computed for a given set of true values by minimizing over the test parameters. This procedure is repeated for all possible true values specified in Table 1.

Sensitivity to the octant of θ_{23} :

This pertains to distinguishing between the LO ($\theta_{23} < \pi/4$) and the HO ($\theta_{23} > \pi/4$). The octant sensitivity at DUNE arises from both $\nu_\mu \rightarrow \nu_e$ and $\nu_\mu \rightarrow \nu_\mu$ channels [72]. To quantify the sensitivity to the octant of θ_{23} , we employ the $\Delta\chi^2$ metric as

$$\Delta\chi_{\text{octant}}^2 = |\chi_{\theta_{23}^{test} > \pi/4}^2 - \chi_{\theta_{23}^{test} < \pi/4}^2|, \quad (14)$$

where, the value of θ_{23} in the wrong octant is constrained to lie strictly within that octant and is not required to match the true value of $\sin^2 2\theta_{23}$.

6 Results and discussion

In this section, we present our results on DUNE sensitivities to CP violation, MH and θ_{23} octant.

Fig. 7 depicts the CP violation sensitivity as a function of true values of CP violating phase, δ_{13} for DUNE TDR (see blue curve) and best reconstruction case (see red curve). The left panel

depicts the $(3+0)$ case while the right panel depicts the $(3+1)$ case. The characteristic double peak shape implies that CP sensitivity is zero at the CP conserving values ($\delta_{13} = 0, \pi$), non-zero at other values ($\delta_{13} \neq 0, \pi$) and peaks at maximal CP violating values ($\delta_{13} = \pm\pi/2$). The best reconstruction case exhibits a statistical advantage over DUNE TDR both in $(3+0)$ and $(3+1)$ cases respectively.

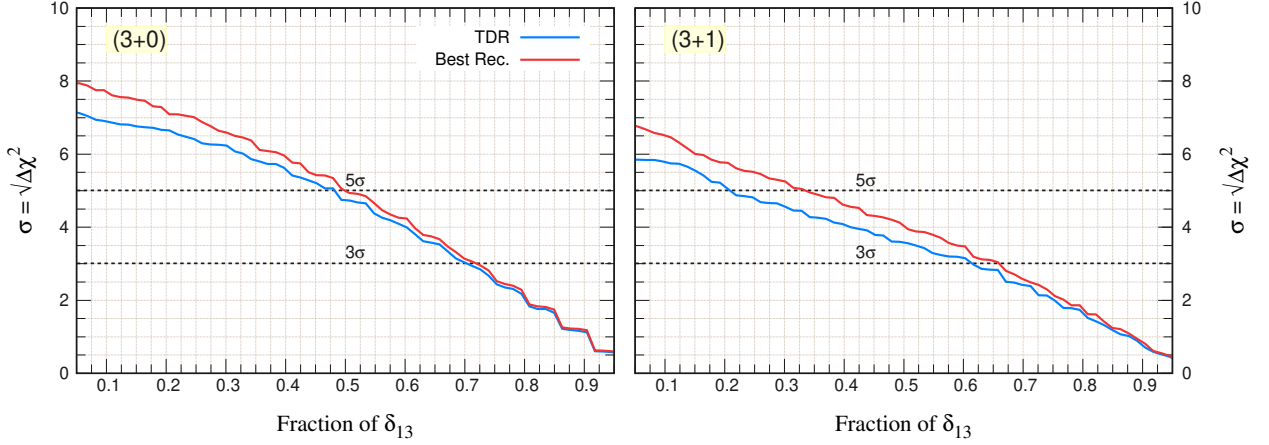


Figure 8: CP violation sensitivity as a function of fraction of δ_{13} for DUNE TDR (blue curve) and best reconstruction (red curve). The left panel depicts the $(3+0)$ case while the right panel depicts the $(3+1)$ case.

The CP violation sensitivity versus fraction of values of δ_{13} for DUNE TDR (blue curve) and the

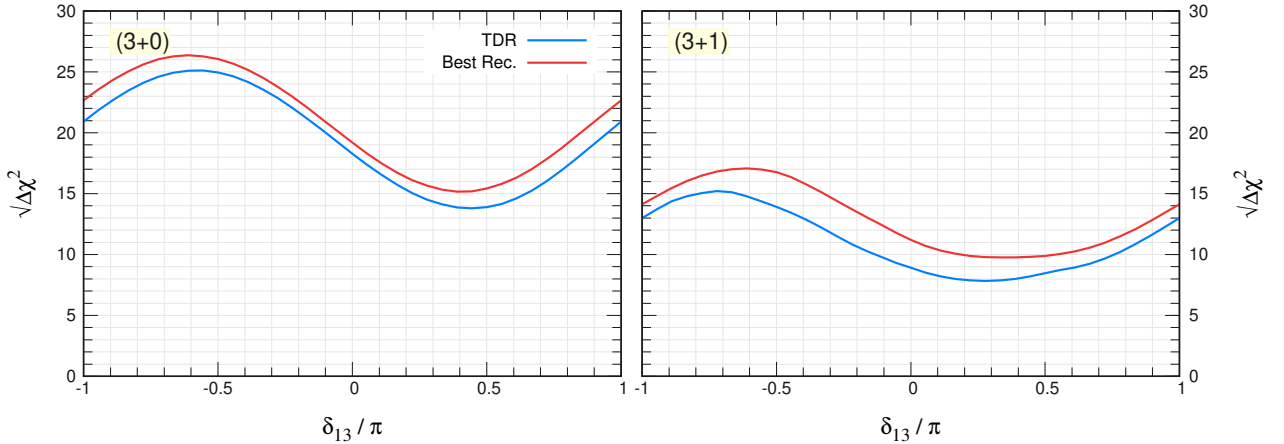


Figure 9: MH sensitivity as a function of δ_{13} for DUNE TDR (blue curve) and best reconstruction scenario (red curve). The left panel depicts the $(3+0)$ case while the right panel depicts the $(3+1)$ case.

best reconstruction case (red curve) is shown in Fig. 8. 5σ (3σ) sensitivity could be achieved by $\sim 48\%$ (71%) and $\sim 50\%$ (73%) values of δ_{13} in $(3+0)$ case with DUNE TDR and best reconstruction scenario respectively. However, for the $(3+0)$ case, we have $\sim 22\%$ (62%) and $\sim 34\%$ (67%) values of δ_{13} with DUNE TDR and best reconstruction scenario respectively.

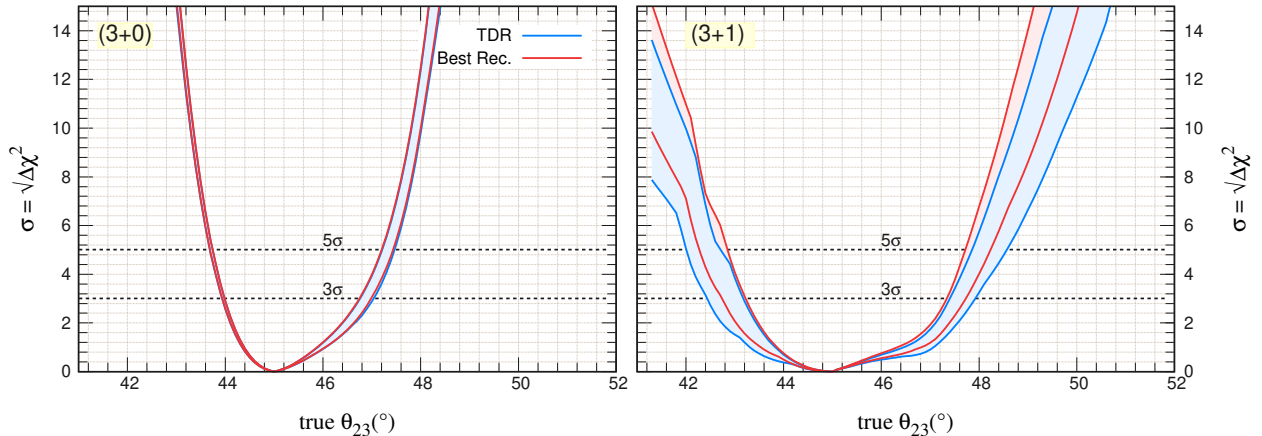


Figure 10: Sensitivity of octant of θ_{23} as a function of θ_{23} for DUNE TDR (blue band) and best reconstruction case (pink band). The left panel depicts the $(3+0)$ case while the right panel depicts the $(3+1)$ case.

Fig. 9 shows the MH sensitivity as a function of true values of δ_{13} with DUNE TDR and best reconstruction case. The MH sensitivity is already high in case of DUNE TDR for all values of the CP phase, δ_{13} in $(3+0)$ case. However, with best reconstruction scenario, sensitivity improves in comparison to DUNE TDR. Similar trend is seen in the $(3+1)$ case.

Fig. 10 shows the sensitivity of determining the octant of θ_{23} as a function of the true values of θ_{23} for DUNE TDR (blue band) and best reconstruction case (pink band). The octant sensitivity is better for θ_{23} lying in the LO for the $(3+0)$ case. The $(3+1)$ case worsens the octant determination but is better for θ_{23} lying in the HO.

7 Conclusion

The key physics goals of the long baseline experiments such as DUNE are to resolve if CP is violated in the leptonic sector, to establish whether the MH is normal or inverted and to figure out what the correct octant of θ_{23} is. In the standard configuration, DUNE would have a total runtime of 13 years (distributed equally in the ν and $\bar{\nu}$ mode) with the standard LE beam. The LE beam that is often used in DUNE simulations has a peak around 2 - 3 GeV but very sharply falls off at $E \gtrsim 4$ GeV. In an earlier work involving some of the authors, we have obtained optimal configuration of runtime and different beam tunes which allow for attaining best sensitivities to these standard unknowns [70]. It has been conclusively shown in literature that any BSM physics scenario such as sterile neutrinos or NSI leads to spoiling of sensitivities of these unknowns [27, 29, 33, 35, 66, 68, 73–77].

It is then interesting to explore the role played by energy resolution and how it impacts DUNE sensitivities in presence of BSM physics. The impact of energy resolution on a particular BSM physics scenario of neutrino NSI has been explored in [43]. In the present work, we have studied the impact of improved energy resolution on DUNE sensitivity to a particular BSM physics scenario of an additional light sterile neutrino, i.e., $(3+1)$ case and compare with results for the standard $(3+0)$ case. Better energy resolution would also aid in disentangling parameter degeneracies among

effects arising from standard three neutrino oscillations ((3 + 0) case) and BSM physics scenario ((3 + 1) case). We consider two cases : standard DUNE TDR and best resolution scenario. As expected using better energy resolution leads to improvement in attaining the key physics goals.

Let us first examine the CP violation sensitivity as depicted in Fig. 7-8 and Table 3. We conclude that with a fixed exposure of 624 kt·MW·yr and nominal energy resolution as given in TDR, DUNE will be able to reach 5σ (3σ) discovery of CP violation for 48% (71%) of δ₁₃ values for (3 + 0) case and 22% (62%) of δ₁₃ values for (3 + 1) case. However, there is improvement with better energy resolution.

The same can be inferred regarding MH (see Fig 9) i.e., with better energy resolution we have improved sensitivity to neutrino MH.

The octant sensitivity is better for θ₂₃ lying in the LO for the (3+0) case. The (3+1) case worsens the octant determination but is better for θ₂₃ lying in the HO (see Fig 10).

Physics goal : CP violation	% of δ ₁₃ values for (3 + 0) case		% of δ ₁₃ values for (3 + 1) case	
	TDR	Best Rec.	TDR	Best Rec.
3σ	71	73	62	67
5σ	48	50	22	34

Table 3: Percentage of δ₁₃ values for which DUNE will achieve 3σ or 5σ CP violation sensitivity for the fixed exposure considered in the present study.

Acknowledgments

SP acknowledges JNU for support in the form of fellowship. The numerical analysis has been performed using the HPC cluster at SPS, JNU funded by DST-FIST. JR would like to thank OSHEC (Odisha State Higher Education Council) for the financial support through Mukhyamantri Research Innovation (MRI) for Extramural Research Funding 2023. The research of PM is supported in part by the International Centre for Theoretical Sciences (ICTS) for participating in the discussion meeting - (QM100) A Hundred Years of Quantum Mechanics (code: ICTS/qm100-2025/01) and by the Inter-University Centre for Astronomy and Astrophysics (IUCAA), Pune through its Associateship Programme.

This work reflects the views of the authors and not those of the DUNE collaboration.

A CP and MH probability differences for the (3 + 0) case

For the (3 + 0) scenario, we use the expressions derived in [53]. In this section, we present the approximate expressions of CP and MH probability differences for ν_μ → ν_e and ν_μ → ν_μ channels. We adopt the parameterization of the mixing matrix as given in Eq. (1).

The CP violating probability differences for ν_μ → ν_e channel, i.e., ΔP_{μe}^{CP(3+0)} is given by

$$\Delta P_{\mu e}^{CP(3+0)} \simeq 4s_{13}^2 s_{23}^2 \left[\frac{\sin^2(\hat{A} - 1)\Delta}{(\hat{A} - 1)^2} - \frac{\sin^2(\hat{A} + 1)\Delta}{(\hat{A} + 1)^2} \right] - 8\alpha s_{13} s_{12} s_{23} c_{12} c_{23} \sin \delta_{13} \\ \frac{\sin \hat{A} \Delta}{\hat{A}} \left[\cos \Delta \cot \delta_{13} \Theta_- + \sin \Delta \Theta_+ \right] + \mathcal{O}(\lambda^4), \quad (\text{A.1})$$

The CP violating probability differences for $\nu_\mu \rightarrow \nu_\mu$ channel, i.e., $\Delta P_{\mu\mu}^{CP(3+0)}$ is given by

$$\begin{aligned}
\Delta P_{\mu\mu}^{CP(3+0)} &\simeq \frac{1}{2\hat{A}}\alpha^2 \sin^2 2\theta_{12} \sin^2 2\theta_{23} \left[\frac{1}{2\hat{A}} \sin 2\hat{A}\Delta \sin 2\Delta - \Delta \sin 2\Delta \right] \\
&+ 4s_{13}^2 s_{23}^2 \left[\frac{\sin^2(\hat{A}+1)\Delta}{(\hat{A}+1)^2} - \frac{\sin^2(\hat{A}-1)\Delta}{(\hat{A}-1)^2} \right] - 2s_{13}^2 \sin^2 2\theta_{23} \left\{ \frac{\hat{A}\Delta}{2} \left(\frac{\sin 2\Delta}{\hat{A}+1} - \frac{\sin 2\Delta}{\hat{A}-1} \right) \right. \\
&+ \left. \sin \Delta \cos \hat{A}\Delta \left(\frac{\sin(\hat{A}+1)\Delta}{(\hat{A}+1)^2} + \frac{\sin(\hat{A}-1)\Delta}{(\hat{A}-1)^2} \right) \right\} \\
&+ 2\alpha s_{13} \sin 2\theta_{12} \sin 2\theta_{23} \cos \delta_{13} \cos \Delta \frac{\sin \hat{A}\Delta}{\hat{A}} \Theta_- \\
&+ 2\alpha s_{13} \sin 2\theta_{12} \sin 2\theta_{23} \cos 2\theta_{23} \cos \delta_{13} \sin \Delta \left\{ \hat{A} \left(\frac{\sin \Delta}{\hat{A}-1} - \frac{\sin \Delta}{\hat{A}+1} \right) \right. \\
&- \left. \frac{\sin \hat{A}\Delta}{\hat{A}} \left(\frac{\cos(\hat{A}+1)\Delta}{\hat{A}+1} + \frac{\cos(\hat{A}-1)\Delta}{\hat{A}-1} \right) \right\} + \mathcal{O}(\lambda^4), \tag{A.2}
\end{aligned}$$

The MH probability differences for $\nu_\mu \rightarrow \nu_e$ channel, i.e., $\Delta P_{\mu e}^{MH(3+0)}$ is given by

$$\begin{aligned}
\Delta P_{\mu e}^{MH(3+0)} &\simeq 4s_{13}^2 s_{23}^2 \left[\frac{\sin^2[\hat{A}-1]\Delta}{(\hat{A}-1)^2} - \frac{\sin^2[\hat{A}+1]\Delta}{(\hat{A}+1)^2} \right] + 2\alpha s_{13} \sin 2\theta_{12} \sin 2\theta_{23} \frac{\sin \hat{A}\Delta}{\hat{A}} \sin \delta_{13} \\
&\left[\Theta_+ \cos \Delta \cot \delta_{13} + \Theta_- \sin \Delta \right] + \mathcal{O}(\lambda^4), \tag{A.3}
\end{aligned}$$

The MH violating probability differences for $\nu_\mu \rightarrow \nu_\mu$ channel, i.e., $\Delta P_{\mu\mu}^{MH(3+0)}$ is given by

$$\begin{aligned}
\Delta P_{\mu\mu}^{MH(3+0)} &\simeq 2\alpha c_{12}^2 \sin^2 2\theta_{23} \Delta \sin 2\Delta + \frac{1}{2\hat{A}}\alpha^2 \sin^2 2\theta_{12} \sin^2 2\theta_{23} \left\{ \frac{\Delta \sin 2\Delta}{\hat{A}} \left[\cos(\hat{A}-1)\Delta \right. \right. \\
&+ \left. \left. \cos(\hat{A}+1)\Delta \right] - \Delta \sin \Delta \right\} + 4s_{13}^2 s_{23}^2 \left[\frac{\sin^2(\hat{A}+1)\Delta}{(\hat{A}+1)^2} - \frac{\sin^2(\hat{A}-1)\Delta}{(\hat{A}-1)^2} \right] \\
&- 2s_{13}^2 \sin^2 2\theta_{23} \left\{ \frac{\hat{A}\Delta}{2} \left[\frac{\sin 2\Delta}{\hat{A}+1} + \frac{\sin 2\Delta}{\hat{A}-1} \right] + \sin \Delta \cos \hat{A}\Delta \left[\frac{\sin(\hat{A}+1)\Delta}{(\hat{A}+1)^2} + \frac{\sin(\hat{A}-1)\Delta}{(\hat{A}-1)^2} \right] \right\} \\
&- 2\alpha s_{13} \sin 2\theta_{12} \sin 2\theta_{23} \cos \delta_{13} \cos \Delta \frac{\sin \hat{A}\Delta}{\hat{A}} \Theta_+ + 2\alpha s_{13} \sin 2\theta_{12} \sin 2\theta_{23} \cos 2\theta_{23} \cos \delta_{13} \sin \Delta \\
&\left\{ \hat{A} \left[\frac{\sin \Delta}{\hat{A}-1} + \frac{\sin \Delta}{\hat{A}+1} \right] + \frac{\sin \hat{A}\Delta}{\hat{A}} \left[\frac{\cos(\hat{A}+1)\Delta}{\hat{A}+1} - \frac{\cos(\hat{A}-1)\Delta}{\hat{A}-1} \right] \right\} + \mathcal{O}(\lambda^4), \tag{A.4}
\end{aligned}$$

where ,

$$\Theta_{\pm} = \left[\frac{\sin(\hat{A}+1)\Delta}{\hat{A}+1} \pm \frac{\sin(\hat{A}-1)\Delta}{\hat{A}-1} \right].$$

References

- [1] T. Kajita and A. B. McDonald. For the discovery of neutrino oscillations, which shows that neutrinos have mass. The Nobel Prize in Physics 2015. <https://www.nobelprize.org/prizes/physics/2015/summary/>.
- [2] P. F. de Salas, D. V. Forero, S. Gariazzo, P. Martínez-Miravé, O. Mena, C. A. Ternes, M. Tórtola, and J. W. F. Valle. 2020 global reassessment of the neutrino oscillation picture. *JHEP*, 02:071, 2021.
- [3] Francesco Capozzi, Eleonora Di Valentino, Eligio Lisi, Antonio Marrone, Alessandro Melchiorri, and Antonio Palazzo. Unfinished fabric of the three neutrino paradigm. *Phys. Rev. D*, 104(8):083031, 2021.
- [4] Ivan Esteban, M. C. Gonzalez-Garcia, Michele Maltoni, Ivan Martinez-Soler, João Paulo Pinheiro, and Thomas Schwetz. NuFit-6.0: Updated global analysis of three-flavor neutrino oscillations. 10 2024.
- [5] Sacha Davidson, Enrico Nardi, and Yosef Nir. Leptogenesis. *Phys. Rept.*, 466:105–177, 2008.
- [6] Carlo Giunti and T. Lasserre. eV-scale Sterile Neutrinos. *Ann. Rev. Nucl. Part. Sci.*, 69:163–190, 2019.
- [7] Basudeb Dasgupta and Joachim Kopp. Sterile Neutrinos. *Phys. Rept.*, 928:1–63, 2021.
- [8] C. Athanassopoulos et al. Evidence for anti-muon-neutrino \rightarrow anti-electron-neutrino oscillations from the LSND experiment at LAMPF. *Phys. Rev. Lett.*, 77:3082–3085, 1996.
- [9] A. A. Aguilar-Arevalo et al. Updated MiniBooNE neutrino oscillation results with increased data and new background studies. *Phys. Rev. D*, 103(5):052002, 2021.
- [10] P. Abratenko et al. First Constraints on Light Sterile Neutrino Oscillations from Combined Appearance and Disappearance Searches with the MicroBooNE Detector. *Phys. Rev. Lett.*, 130(1):011801, 2023.
- [11] A. A. Aguilar-Arevalo et al. MiniBooNE and MicroBooNE Combined Fit to a 3+1 Sterile Neutrino Scenario. *Phys. Rev. Lett.*, 129(20):201801, 2022.
- [12] J. N. Abdurashitov et al. Measurement of the solar neutrino capture rate with gallium metal. III: Results for the 2002–2007 data-taking period. *Phys. Rev. C*, 80:015807, 2009.
- [13] F. Kaether, W. Hampel, G. Heusser, J. Kiko, and T. Kirsten. Reanalysis of the GALLEX solar neutrino flux and source experiments. *Phys. Lett. B*, 685:47–54, 2010.
- [14] V. V. Barinov et al. Results from the Baksan Experiment on Sterile Transitions (BEST). *Phys. Rev. Lett.*, 128(23):232501, 2022.
- [15] Patrick Huber. On the determination of anti-neutrino spectra from nuclear reactors. *Phys. Rev. C*, 84:024617, 2011. [Erratum: *Phys.Rev.C* 85, 029901 (2012)].
- [16] G. Mention, M. Fechner, Th. Lasserre, Th. A. Mueller, D. Lhuillier, M. Cribier, and A. Letourneau. The Reactor Antineutrino Anomaly. *Phys. Rev. D*, 83:073006, 2011.
- [17] A. P. Serebrov et al. Search for sterile neutrinos with the Neutrino-4 experiment and measurement results. *Phys. Rev. D*, 104(3):032003, 2021.

- [18] Pedro AN Machado, Ornella Palamara, and David W Schmitz. The Short-Baseline Neutrino Program at Fermilab. *Ann. Rev. Nucl. Part. Sci.*, 69:363–387, 2019.
- [19] P. Abratenko et al. Scintillation light in SBND: simulation, reconstruction, and expected performance of the photon detection system. *Eur. Phys. J. C*, 84(10):1046, 2024.
- [20] D. Torretta. Status and perspectives of the ICARUS experiment at the Fermilab Short Baseline Neutrino program. *JINST*, 19(04):C04061, 2024.
- [21] K. Abe et al. Hyper-Kamiokande Design Report. *arXiv:1805.04163*.
- [22] Babak Abi et al. Deep Underground Neutrino Experiment (DUNE), Far Detector Technical Design Report, Volume II: DUNE Physics. 2 2020.
- [23] B. Abi et al. Experiment Simulation Configurations Approximating DUNE TDR. *arXiv:2103.04797*.
- [24] A. V. Akhondov et al. Letter of Interest for a Neutrino Beam from Protvino to KM3NeT/ORCA. *Eur. Phys. J. C*, 79(9):758, 2019.
- [25] S. Adrian-Martinez et al. Letter of intent for KM3NeT 2.0. *J. Phys. G*, 43(8):084001, 2016.
- [26] Srubabati Goswami. Accelerator, reactor, solar and atmospheric neutrino oscillation: Beyond three generations. *Phys. Rev. D*, 55:2931–2949, 1997.
- [27] Raj Gandhi, Boris Kayser, Mehedi Masud, and Suprabh Prakash. The impact of sterile neutrinos on CP measurements at long baselines. *JHEP*, 11:039, 2015.
- [28] Stephen Parke and Mark Ross-Lonergan. Unitarity and the three flavor neutrino mixing matrix. *Phys. Rev. D*, 93(11):113009, 2016.
- [29] Debajyoti Dutta, Raj Gandhi, Boris Kayser, Mehedi Masud, and Suprabh Prakash. Capabilities of long-baseline experiments in the presence of a sterile neutrino. *JHEP*, 11:122, 2016.
- [30] Raj Gandhi, Boris Kayser, Suprabh Prakash, and Samiran Roy. What measurements of neutrino neutral current events can reveal. *JHEP*, 11:202, 2017.
- [31] T. S. Kosmas, D. K. Papoulias, M. Tortola, and J. W. F. Valle. Probing light sterile neutrino signatures at reactor and Spallation Neutron Source neutrino experiments. *Phys. Rev. D*, 96(6):063013, 2017.
- [32] Sandhya Choubey, Debajyoti Dutta, and Dipyaman Pramanik. Imprints of a light Sterile Neutrino at DUNE, T2HK and T2HKK. *Phys. Rev. D*, 96(5):056026, 2017.
- [33] Sanjib Kumar Agarwalla, Sabya Sachi Chatterjee, and Antonio Palazzo. Signatures of a Light Sterile Neutrino in T2HK. *JHEP*, 04:091, 2018.
- [34] Yakefu Reyimuaji and Chun Liu. Prospects of light sterile neutrino searches in long-baseline neutrino oscillations. *JHEP*, 06:094, 2020.
- [35] Animesh Chatterjee, Srubabati Goswami, and Supriya Pan. Matter effect in presence of a sterile neutrino and resolution of the octant degeneracy using a liquid argon detector. *Phys. Rev. D*, 108(9):095050, 2023.

- [36] Dinesh Kumar Singha, Monojit Ghosh, Rudra Majhi, and Rukmani Mohanta. Study of light sterile neutrino at the long-baseline experiment options at KM3NeT. *Phys. Rev. D*, 107(7):075039, 2023.
- [37] Dibya S. Chattopadhyay, Moon Moon Devi, Amol Dighe, Debajyoti Dutta, Dipyaman Pramanik, and Sushant K. Raut. Sterile neutrinos: propagation in matter and sensitivity to sterile mass ordering. *JHEP*, 02:044, 2023.
- [38] Rudra Majhi, C. Soumya, and Rukmani Mohanta. Light sterile neutrinos and their implications on currently running long-baseline and neutrinoless double beta decay experiments. *J. Phys. G*, 47(9):095002, 2020.
- [39] Nishat Fiza, Mehedi Masud, and Manimala Mitra. Exploring the new physics phases in 3+1 scenario in neutrino oscillation experiments. *JHEP*, 09:162, 2021.
- [40] Sabila Parveen, Kiran Sharma, Sudhanwa Patra, and Poonam Mehta. Signals of eV-scale sterile neutrino at long baseline neutrino experiments. *Eur. Phys. J. C*, 85(2):181, 2025.
- [41] Sabila Parveen, Mehedi Masud, Mary Bishai, and Poonam Mehta. Sterile sector impacting the correlations and degeneracies among mixing parameters at the Deep Underground Neutrino Experiment. *JHEP*, 01:139, 2025.
- [42] Valentina De Romeri, Enrique Fernandez-Martinez, and Michel Sorel. Neutrino oscillations at DUNE with improved energy reconstruction. *JHEP*, 09:030, 2016.
- [43] Sabya Sachi Chatterjee, P. S. Bhupal Dev, and Pedro A. N. Machado. Impact of improved energy resolution on DUNE sensitivity to neutrino non-standard interactions. *JHEP*, 08:163, 2021.
- [44] B. Pontecorvo. Inverse beta processes and nonconservation of lepton charge. *Zh. Eksp. Teor. Fiz.*, 34:247, 1957.
- [45] B. Pontecorvo. Mesonium and anti-mesonium. *Sov. Phys. JETP*, 6:429, 1957.
- [46] Ziro Maki, Masami Nakagawa, and Shoichi Sakata. Remarks on the unified model of elementary particles. *Prog. Theor. Phys.*, 28:870–880, 1962.
- [47] V.N. Gribov and B. Pontecorvo. Neutrino astronomy and lepton charge. *Phys. Lett. B*, 28:493, 1969.
- [48] S. Navas et al. Review of particle physics. *Phys. Rev. D*, 110(3):030001, 2024.
- [49] Joachim Kopp, Pedro A. N. Machado, Michele Maltoni, and Thomas Schwetz. Sterile Neutrino Oscillations: The Global Picture. *JHEP*, 05:050, 2013.
- [50] N. Klop and A. Palazzo. Imprints of CP violation induced by sterile neutrinos in T2K data. *Phys. Rev. D*, 91(7):073017, 2015.
- [51] B. Abi et al. Prospects for beyond the Standard Model physics searches at the Deep Underground Neutrino Experiment. *Eur. Phys. J. C*, 81(4):322, 2021.
- [52] Mona Dentler, Álvaro Hernández-Cabezudo, Joachim Kopp, Pedro A. N. Machado, Michele Maltoni, Ivan Martinez-Soler, and Thomas Schwetz. Updated Global Analysis of Neutrino Oscillations in the Presence of eV-Scale Sterile Neutrinos. *JHEP*, 08:010, 2018.

- [53] Evgeny K. Akhmedov, Robert Johansson, Manfred Lindner, Tommy Ohlsson, and Thomas Schwetz. Series expansions for three flavor neutrino oscillation probabilities in matter. *JHEP*, 04:078, 2004.
- [54] Patrick Huber, M. Lindner, and W. Winter. Simulation of long-baseline neutrino oscillation experiments with GLOBES (General Long Baseline Experiment Simulator). *Comput. Phys. Commun.*, 167:195, 2005.
- [55] Patrick Huber, Joachim Kopp, Manfred Lindner, Mark Rolinec, and Walter Winter. New features in the simulation of neutrino oscillation experiments with GLOBES 3.0: General Long Baseline Experiment Simulator. *Comput. Phys. Commun.*, 177:432–438, 2007.
- [56] A. M. Dziewonski and D. L. Anderson. Preliminary reference earth model. *Phys. Earth Planet. Interiors*, 25:297–356, 1981.
- [57] S. Agostinelli et al. GEANT4: A Simulation toolkit. *Nucl. Instrum. Meth.*, A506:250–303, 2003.
- [58] John Allison et al. Geant4 developments and applications. *IEEE Trans. Nucl. Sci.*, 53:270, 2006.
- [59] Raj Gandhi, Pomita Ghoshal, Srubabati Goswami, Poonam Mehta, and S. Uma Sankar. Large matter effects in $\nu(\mu) \rightarrow \nu(\tau)$ oscillations. *Phys. Rev. Lett.*, 94:051801, 2005.
- [60] Raj Gandhi, Pomita Ghoshal, Srubabati Goswami, Poonam Mehta, and S. Uma Sankar. Earth matter effects at very long baselines and the neutrino mass hierarchy. *Phys. Rev. D*, 73:053001, 2006.
- [61] Kevin J. Kelly and Stephen J. Parke. Matter Density Profile Shape Effects at DUNE. *Phys. Rev. D*, 98(1):015025, 2018.
- [62] Animesh Chatterjee, Felipe Kamiya, Celio A. Moura, and Jaehoon Yu. Impact of Matter Density Profile Shape on Non-Standard Interactions at DUNE. *arXiv:1809.09313*.
- [63] B. Abi et al. Deep underground neutrino experiment (dune), far detector technical design report, volume i: Introduction to dune. *JINST*, 15:T08008, 2020.
- [64] Alexander Friedland and Shirley Weishi Li. Understanding the energy resolution of liquid argon neutrino detectors. *Phys. Rev. D*, 99(3):036009, 2019.
- [65] M. Bass et al. Baseline Optimization for the Measurement of CP Violation, Mass Hierarchy, and θ_{23} Octant in a Long-Baseline Neutrino Oscillation Experiment. *Phys. Rev. D*, 91(5):052015, 2015.
- [66] Mehedi Masud and Poonam Mehta. Nonstandard interactions and resolving the ordering of neutrino masses at DUNE and other long baseline experiments. *Phys. Rev. D*, 94(5):053007, 2016.
- [67] Mark D. Messier. *Evidence for neutrino mass from observations of atmospheric neutrinos with Super-Kamiokande*. PhD thesis, Boston U., 1999.
- [68] Mehedi Masud, Animesh Chatterjee, and Poonam Mehta. Probing CP violation signal at DUNE in presence of non-standard neutrino interactions. *J. Phys. G*, 43(9):095005, 2016.

- [69] Jogesh Rout, Sheeba Shafaq, Mary Bishai, and Poonam Mehta. Physics prospects with the second oscillation maximum at the Deep Underground Neutrino Experiment. *Phys. Rev. D*, 103(11):116003, 2021.
- [70] Jogesh Rout, Samiran Roy, Mehedi Masud, Mary Bishai, and Poonam Mehta. Impact of high energy beam tunes on the sensitivities to the standard unknowns at DUNE. *Phys. Rev. D*, 102:116018, 2020.
- [71] X. Qian, A. Tan, W. Wang, J. J. Ling, R. D. McKeown, and C. Zhang. Statistical Evaluation of Experimental Determinations of Neutrino Mass Hierarchy. *Phys. Rev.*, D86:113011, 2012.
- [72] R. Acciarri et al. Long-Baseline Neutrino Facility (LBNF) and Deep Underground Neutrino Experiment (DUNE): Conceptual Design Report, Volume 2: The Physics Program for DUNE at LBNF. 12 2015.
- [73] André de Gouvêa and Kevin J. Kelly. Non-standard neutrino interactions at DUNE. *Nucl. Phys. B*, 908:318–335, 2016.
- [74] Pilar Coloma. Non-Standard Interactions in propagation at the Deep Underground Neutrino Experiment. *JHEP*, 03:016, 2016.
- [75] Sanjib Kumar Agarwalla, Sabya Sachi Chatterjee, and Antonio Palazzo. Octant of θ_{23} in danger with a light sterile neutrino. *Phys. Rev. Lett.*, 118(3):031804, 2017.
- [76] Francesco Capozzi, Sabya Sachi Chatterjee, and Antonio Palazzo. Neutrino Mass Ordering Obscured by Nonstandard Interactions. *Phys. Rev. Lett.*, 124(11):111801, 2020.
- [77] Sabya Sachi Chatterjee and Antonio Palazzo. Nonstandard Neutrino Interactions as a Solution to the $NO\nu A$ and T2K Discrepancy. *Phys. Rev. Lett.*, 126(5):051802, 2021.